DOI 10.1007/s10778-014-0640-z
International Applied Mechanics, Vol. 50, No. 4, July, 2014

THREE-DIMENSIONAL ANALYSIS OF THE LOWER FREQUENCIES OF A CANTILEVERED ANISOTROPIC PARALLELEPIPED

E. I. Bespalova and G. P. Urusova

An approach to determining the lower frequencies of a cantilevered elastic parallelepiped using a three-dimensional problem statement and allowing for material anisotropy is developed. The approach combines the inverse-iteration and extended Kantorovich–Vlasov methods and is validated against the combination of the finite-element and Ritz methods. The influence of the anisotropy of the material on the lower frequencies of the parallelepiped is analyzed. It is shown that the variation in the frequencies of the parallelepiped with the boundary conditions being considered follows the variation in the predominant stiffness characteristics

Keywords: elastic parallelepiped, cantilever, different types of anisotropy, three-dimensional problem statement, natural frequencies, extended Kantorovich–Vlasov method

Introduction. Cantilevered elastic members of various shape and structure are widely used in various fields of engineering and construction. They are used to model wings of aircraft and blades of gas-turbine engines in mechanical engineering; elements of floors of buildings, balcony girders, and multistorey structures in construction; elements of scanning electron microscopes in nanoelectromechanical systems. No wonder that cantilever restraint is deemed to be a technological masterpiece. An analysis of the vibrations of such members is an important initial stage in their dynamic design, which may prevent emergencies under real service conditions.

By now, the dynamic characteristics of cantilevered elastic members have been most extensively studied for beams and thin plates either of simple structure or with some complicating factors. For example, the influence of lamination of beams on their vibrations was studied in [9], the dependence of the lower frequencies on the elastic properties of composites was analyzed in [20], and discrete inclusions such as lumped masses were allowed for in [8]. We will use beam models, the classical Kirchhoff–Love model, and shear models of the first and higher orders.

The vibrations of cantilevered bodies have been studied, using a three-dimensional problem statement, mainly for thick plates of various shapes such as an isosceles triangle, a rectangular parallelepiped, a prism with skew edge opposite to fixed one, etc. [18, 19, 21, 22]. The three-dimensional problem statement in elasticity was compared in [18] with different two-dimensional problem statements for plates depending on their geometrical parameters. Particular attention was given to the boundary conditions on the lateral faces, and the frequency analysis was usually restricted to the case of an isotropic material [19]. The free vibrations of thick anisotropic plates were studied in few publications. The lower frequencies of square plates of different thickness made of materials with different types of anisotropy were analyzed in [3]. Various combinations of boundary conditions on the lateral faces, except for the cantilever case, were considered.

To solve the relevant two- and three-dimensional eigenvalue problems, use is often made of variational difference and finite-element methods as well as discrete-continuous and Ritz methods [3, 12, 14, 17–19, 21]. The frequencies of an isotropic parallelepiped obtained by the Ritz method using various basis functions (algebraic and Chebyshev polynomials, trigonometric functions, etc.) were compared in detail in [19]. It was pointed out that B-splines are promising for achieving high accuracy. The

S. P. Timoshenko Institute of Mechanics, National Academy of Sciences of Ukraine, 3 Nesterova St., Kyiv, Ukraine 03057, e-mail: metod@inmech.kiev.ua. Translated from Prikladnaya Mekhanika, Vol. 50, No. 4, pp. 16–29, July–August 2014. Original article submitted December 5, 2011.

spline-collocation method was used to study the free axisymmetric vibrations of solid cylinders with either clamped or sliding ends [11] and to solve a three-dimensional static problem for a thick plate with the same boundary conditions [13]. Finite integral transforms were used in [15] to analyze the stress–strain state of cantilevered thin orthotropic plates under arbitrary loading. Some two-dimensional problems were solved by the superposition method [10] Three-dimensional eigenvalue problems for an isotropic parallelepiped were solved by the extended Kantorovich–Vlasov method [6]. The same method was used to study the torsion of a rectangular anisotropic prism [5], to solve the Lame problem of the compression of an elastic parallelepiped [7], and to solve two-dimensional stationary problems for shallow shells [4].

Here we will analyze the natural frequencies of cantilevered parallelepipeds with different dimensions made of materials with different types of anisotropy. To solve the associated problems, we will combine the inverse-iteration and extended Kantorovich–Vlasov methods.

1. Problem Statement and Problem-Solving Method. Consider an elastic body in the form of a rectangular parallelepiped occupying a domain $\Omega \cup \partial\Omega = \{x, y, z: x \in [0, a],\ y \in [0, b],\ z \in [0,\ c]\}$ in Cartesian coordinates x, y, z. The body is cantilevered: the edge $x = 0$ is clamped, and the other edges are free. In the general case, various physically consistent boundary conditions may be prescribed on the faces of the body.

The problem of the free vibrations of the parallelepiped is formulated using the Rayleigh variational principle:

$$\delta\Im(\overline{U}, \lambda) = \delta(\Pi(\overline{U}) - \lambda K(\overline{U})) = 0, \tag{1.1}$$

where $\Pi(\overline{U}) = \frac{1}{2}\int\limits_{\Omega} (D\overline{U})^T C D\overline{U} d\hat{\omega}$ and $K(\overline{U}) = \frac{1}{2}\int\limits_{\Omega} \overline{U}^T \rho \overline{U} d\hat{\omega}$ are the potential and kinetic energies of the body; λ is the Lagrange multiplier (squared natural frequency),

$$\lambda = \omega^2 = \frac{\Pi}{K} = \frac{\int\limits_{\Omega} (D\overline{U})^T C D\overline{U} d\hat{\omega}}{\int\limits_{\Omega} \overline{U}^T \rho \overline{U} d\hat{\omega}} \quad \text{(Rayleigh relation);} \tag{1.2}$$

$\overline{U} = \{u_p(x, y, z)\}_{p=x,\ y,\ z}$ is the displacement vector of particles of the body; D is a matrix differential operator,

$$D = \begin{pmatrix} \partial/\partial x & 0 & 0 \\ 0 & \partial/\partial y & 0 \\ 0 & 0 & \partial/\partial z \\ 0 & \partial/\partial z & \partial/\partial y \\ \partial/\partial z & 0 & \partial/\partial x \\ \partial/\partial y & \partial/\partial x & 0 \end{pmatrix},$$

$C = \{c_{ij}\}$ $(i, j = \overline{1, 6})$ is the matrix of elastic constants of the generalized Hooke's law $\overline{\sigma} = C\overline{\varepsilon}$ for an anisotropic material ($\overline{\sigma} = \{\sigma_{11}, \sigma_{22}, \sigma_{33}, \sigma_{23}, \sigma_{13}, \sigma_{12}\}$ and $\overline{\varepsilon} = \{\varepsilon_{11}, \varepsilon_{22}, \varepsilon_{33}, \varepsilon_{23}, \varepsilon_{13}, \varepsilon_{12}\}$ are the stress and strain vectors composed of the elements of the respective tensors with allowance for their symmetry); $\rho = \rho(x, y, z)$ is the mass distribution function; $\hat{\omega}$ is a volume element Ω (the indices 1, 2, 3 correspond to x, y, z, all the vectors being column vectors).

The unknown parameter λ and the associated state $\overline{U}$ (1.1) are determined, as in [6], by combining the inverse-iteration method [1] and the extended Kantorovich–Vlasov (EKM) method [4, 5].

First, we use the method of successive approximations to reduce problem (1.1) to a sequence of variational problems that do not contain the unknown factor λ. To this end, we introduce a sequence of vector functions $\overline{V}^n$ as $\overline{U} = \overline{V}^n$ and $\lambda\overline{U} = \overline{V}^{n-1}$ to reduce the original problem to a sequence of variational problems for the functionals

$$\Im(\overline{U}, \lambda) \to \Im_n(\overline{V}^n) = \frac{1}{2}\int\limits_{\Omega} (D\overline{V}^n)^T C D\overline{V}^n d\hat{\omega} - \frac{1}{2}\tau\int\limits_{\Omega} (\overline{V}^n)^T \rho \overline{V}^n d\omega - \frac{1}{2}\int\limits_{\Omega} (\overline{V}^n)^T \rho \overline{V}^{n-1} d\hat{\omega}, \tag{1.3}$$

and the factor λ is determined as the limit of the following numerical sequence:

$$\lambda_n = \frac{\Pi_n}{K_n} = \frac{\int\limits_{\Omega} \left((D\bar{V}^n)^T C D \bar{V}^n - \tau (\bar{V}^n)^T \rho \bar{V}^n \right) d\hat{\omega}}{\int\limits_{\Omega} (\bar{V}^n)^T \rho \bar{V}^n d\hat{\omega}} \quad (n = 1, 2, \ldots). \tag{1.4}$$

It is necessary to take into account the shift of the eigenvalue spectrum by τ ($\lambda \to \lambda + \tau$).

Any vector function of general form can be used as the initial approximation $\bar{V}^0$.

To find the stationary points of functional (1.3) at some fixed step $n - fixed$, we will use the method based on the extended Kantorovich–Vlasov method and detailed in [5]. This method suggests approximating the displacement vector $\bar{V}^n = \{v_1^n, v_2^n, v_3^n\}$ in functional (1.3) by a vector $\bar{F}_M^n = \{f_{1M}^n, f_{2M}^n, f_{3M}^n\}$ as follows:

$$v_1^n(x,y,z) \simeq f_{1M}^n(x,y,z) = \sum_{i=1}^{M} X_{1i}^n(x) Y_{1i}^n(y) Z_{1i}^n(z),$$

$$v_2^n(x,y,z) \simeq f_{2M}^n(x,y,z) = \sum_{i=1}^{M} X_{2i}^n(x) Y_{2i}^n(y) Z_{2i}^n(z),$$

$$v_3^n(x,y,z) \simeq f_{3M}^n(x,y,z) = \sum_{i=1}^{M} X_{3i}^n(x) Y_{3i}^n(y) Z_{3i}^n(z), \tag{1.5}$$

where the functions $X_{1i}^n(x), X_{2i}^n(x), X_{3i}^n(x), Y_{1i}^n(y), Y_{2i}^n(y), Y_{3i}^n, Z_{1i}^n(z), Z_{2i}^n(z), Z_{3i}^n(z)$ ($i = \overline{1, M}$) depend on different variables of the domain Ω and are unknown; M is the number of terms in the approximating expression.

For convenience, we will represent these functions as elements of the following vectors:

$$\bar{X}^n = \{X_{\pi}^n(x)\}_{\substack{p=1,2,3; \\ i=\overline{1,M}}} = \{X_{11}^n(x) \ldots X_{21}^n(x) \ldots X_{31}^n(x) \ldots X_{3M}^n(x)\}, \tag{1.6}$$

$$\bar{Y}^n = \{Y_{\pi}^n(y)\}_{\substack{p=1,2,3; \\ i=\overline{1,M}}} = \{Y_{11}^n(y) \ldots Y_{21}^n(y) \ldots Y_{31}^n(y) \ldots Y_{3M}^n(y)\}, \tag{1.7}$$

$$\bar{Z}^n = \{Z_{\pi}^n(z)\}_{\substack{p=1,2,3; \\ i=\overline{1,M}}} = \{Z_{11}^n(z) \ldots Z_{21}^n(z) \ldots Z_{31}^n(z) \ldots Z_{3M}^n(z)\}. \tag{1.8}$$

These vectors, as in [4–7], are said to be argument vector functions since each of them is composed of functions of only one argument x, y, or z. To determine them, we use the standard procedure of variational calculus. For example, according to the approximation $\bar{F}_M^n = \{f_{1M}^n, f_{2M}^n, f_{3M}^n\}$ (1.5), functional (1.3) is approximately replaced by the functional

$$\Im_n(\bar{V}^n) \cong \Im_{nM}(\bar{F}_M^n) = \Im_{nM}(\bar{X}^n, \bar{Y}^n, \bar{Z}^n) = \frac{1}{2} \int_{\Omega} (D\bar{F}_M^n)^T C D \bar{F}_M^n d\hat{\omega} - \frac{1}{2} \int_{\Omega} (\bar{F}_M^n)^T \rho \bar{F}_M^{n-1} d\hat{\omega}.$$

The stationarity condition for this functional is

$$\delta \Im_{nM}(\bar{X}^n, \bar{Y}^n, \bar{Z}^n) = \delta_{\bar{X}^n} \Im_{nM} \delta \bar{X}^n + \delta_{\bar{Y}^n} \Im_{nM} \delta \bar{Y}^n + \delta_{\bar{Z}^n} \Im_{nM} \delta \bar{Z}^n = 0, \tag{1.9}$$

where $\delta_{\bar{X}^n} \Im_{nM}, \delta_{\bar{Y}^n} \Im_{nM}, \delta_{\bar{Z}^n} \Im_{nM}$ are partial variations of the functional $\Im_{nM}$ with respect to the elements of the vectors $\bar{X}^n$, $\bar{Y}^n, \bar{Z}^n$, respectively. Since the vectors $\bar{X}^n, \bar{Y}^n, \bar{Z}^n$ are independent, condition (1.9) is equivalent to the following conditions:

$$\delta_{\bar{X}^n} \Im_{nM} = \sum_{k=1}^{M} (\delta_{X_{1k}^n} \Im_{nM} \delta X_{1k}^n + \delta_{X_{2k}^n} \Im_{nM} \delta X_{2k}^n + \delta_{X_{3k}^n} \Im_{nM} \delta X_{3k}^n) = 0, \tag{1.10}$$

$$\delta_{\overline{Y}^n} \Im_{nM} = \sum_{k=1}^{M} (\delta_{Y_{1k}^n} \Im_{nM} \delta Y_{1k}^n + \delta_{Y_{2k}^n} \Im_{nM} \delta Y_{2k}^n + \delta_{Y_{3k}^n} \Im_{nM} \delta Y_{3k}^n) = 0, \tag{1.11}$$

$$\delta_{\overline{Z}^n} \Im_{nM} = \sum_{k=1}^{M} (\delta_{Z_{1k}^n} \Im_{nM} \delta Z_{1k}^n + \delta_{Z_{2k}^n} \Im_{nM} \delta Z_{2k}^n + \delta_{Z_{3k}^n} \Im_{nM} \delta Z_{3k}^n) = 0. \tag{1.12}$$

When going over to the Euler–Lagrange equations, each of conditions (1.10)–(1.12) generates a one-dimensional problem for a varied argument vector function. The argument functions of other variables that are not varied in this condition appear in this one-dimensional problem as parameter functionals. A procedure of deriving these one-dimensional problems is outlined in [5]. For example, the one-dimensional problem for the functions $\overline{X}^n$ with respect to the variable x is equivalent to condition (1.10), while the functions $\overline{Y}^n$ and $\overline{Z}^n$ appear in it as definite integrals. Condition (1.11) leads to a one-dimensional problem for the functions $\overline{Y}^n$ with respect to the variable y, while the functions $\overline{X}^n$ and $\overline{Z}^n$ appear in it as definite integrals. The one-dimensional problem for the vector function $\overline{Z}^n$ with respect to the variable z follows from condition (1.12) and includes the functions $\overline{X}^n$ and $\overline{Y}^n$ in integral form. Thus, the system of conditions (1.10)–(1.12) leads to the following system of three one-dimensional boundary-value problems with respect to three argument vector functions of different variables:

$$(L_x^n - \tau T_x^n)\overline{X}^n - T_x^n \overline{X}^{n-1} = 0, \quad x \in (0, a); \quad R_{\mp x}^n \overline{X}^n = 0, \quad x = 0, a, \tag{1.13}$$

$$(L_y^n - \tau T_y^n)\overline{Y}^n - T_y^n \overline{Y}^{n-1} = 0, \quad y \in (0, b); \quad R_{\mp y}^n \overline{Y}^{(n)} = 0, \quad y = 0, b, \tag{1.14}$$

$$(L_z^n - \tau T_z^n)\overline{Z}^n - T_z^n \overline{Z}^{n-1} = 0, \quad z \in (0, c); \quad R_{\mp z}^n \overline{Z}^n = 0, \quad z = 0, c, \tag{1.15}$$

where $L_x^n = \{l_{sp}\}_{s,p=1,2,3}$ is a block matrix whose blocks $l_{sp} = \{l_{ik}^{sp}\}_{i,k=\overline{1,M}}$ are matrix differential operators of the second order with respect to the variable x:

$$l_{ik}^{sp} = A_{2ik}^{sp} \frac{d^2}{dx^2} + A_{1ik}^{sp} \frac{d}{dx} + A_{0ik}^{sp}, \tag{1.16}$$

$T_x^n = \{t_{ik}^{ss}\}_{\substack{s=1,2,3 \\ i,k=\overline{1,M}}}$ is a block-diagonal matrix.

The matrix operator of boundary conditions (the sign "–" refers to $x = 0$, and the sign "+" to $x = a$) is expressed in a similar way:

$$R_{\mp x}^n = \left\{ r_{\mp ik}^{sp} = r_{\mp 1ik}^{sp} \frac{d}{dx} + r_{\mp 0ik}^{sp} \right\}.$$

The coefficients of operators (1.16) in the case of general rectilinear anisotropy can be found in [5].

The block-diagonal matrix $T_x^n = \{t_{ik}^{ss}\}_{\substack{s=1,2,3 \\ i,k=\overline{1,M}}}$ has the following elements:

$$t_{ik}^{11} = \int_0^b \int_0^c \rho Y_{1i} Y_{1k} Z_{1i} Z_{1k} \, dydz, \quad t_{ik}^{22} = \int_0^b \int_0^c \rho Y_{2i} Y_{2k} Z_{2i} Z_{2k} \, dydz, \quad t_{ik}^{33} = \int_0^b \int_0^c \rho Y_{3i} Y_{3k} Z_{3i} Z_{3k} \, dydz.$$

The elements of the matrices T_y^n and T_z^n are similar.

To solve the system of one-dimensional problems (1.13)–(1.15) at each step of the method of successive approximations (parameter n), the following iteration scheme (parameter m) can be used:

$$(L_x^{n,m-1} - \tau T_x^{n,m-1})\overline{X}^{n,m} - T_x^{n,m-1} \overline{X}^{n-1,m-1} = 0, \quad x \in (0, a); \quad R_{\mp x}^{n,m-1} \overline{X}^{n,m} = 0, \quad x = 0, a, \tag{1.17}$$

$$(L_y^{n,m-1} - \tau T_y^{n,m-1})\bar{Y}^{n,m} - T_y^{n,m-1}\bar{Y}^{n-1,m-1} = 0, \quad y \in (0, b); \quad R_{\mp y}^{n,m-1}\bar{Y}^{n,m} = 0, \quad y = 0, b, \tag{1.18}$$

$$(L_z^{n,m} - \tau T_z^{n,m})\bar{Z}^{n,m} - T_z^{n,m}\bar{Z}^{n-1,m-1} = 0, \quad z \in (0, c); \quad R_{\mp z}^{n,m}\bar{Z}^{n,m} = 0, \quad z = 0, c$$

$$(m = 1, 2, \ldots). \tag{1.19}$$

The index $(m-1)$ on the operators $L_x^{n,m-1}$, $T_x^{n,m-1}$, $R_{\mp x}^{n,m-1}$ means that the coefficients are calculated using the functions Y and Z from the previous $(m-1)$th step of approximation. These indices have the same meaning in the other operators of (1.17)–(1.19).

Thus, as in solving the analogous problem for an isotropic parallelepiped [6], we set up a single iteration process (parameter $j = 1, 2, \ldots$) to determine the frequency parameter λ and the associated vector function $\bar{U}$. This process unites inverse iterations (parameter n) and solution of the variational problem (1.17)–(1.19) (parameter m):

$$(L_x^{j-1} - \tau T_x^{j-1})\bar{X}^j - T_x^{j-1}\bar{X}^{j-1} = 0, \quad x \in (0, a); \quad R_{\mp x}^{j-1}\bar{X}^j = 0, \quad x = 0, a, \tag{1.20}$$

$$(L_y^{j-1} - \tau T_y^{j-1})\bar{Y}^j - T_y^{j-1}\bar{Y}^{j-1} = 0, \quad y \in (0, b); \quad R_{\mp y}^{j-1}\bar{Y}^j = 0, \quad y = 0, b, \tag{1.21}$$

$$(L_z^j - \tau T_z^j)\bar{Z}^j - T_z^j\bar{Z}^{j-1} = 0, \quad z \in (0, c); \quad R_{\mp z}^j\bar{Z}^j = 0, \quad z = 0, c. \tag{1.22}$$

Note that any functions linearly independent in i may be chosen as the initial approximations X_{pi}^0, Y_{pi}^0, Z_{pi}^0 ($p = 1, 2, 3$, $i = \overline{1, M}$). Each one-dimensional boundary-value problem is solved by the orthogonal-sweep method.

To terminate the iteration process (1.20)–(1.22) with a fixed number M of approximation terms, we will use the Runge principle. The accuracy of the calculated natural frequency λ is improved by increasing the number of terms M in (1.5).

2. Test Example. Since the method for solving three-dimensional eigenvalue problems has not yet been rigorously validated (no deductive estimation of the convergence and accuracy of the solution has been done), its practical justification as applied to spectral problems of elasticity for anisotropic bodies is based on the well-known inductive techniques of applied mathematics.

As follows from Sec. 1, to solve the problem, it is necessary that the following two conditions be satisfied: (i) convergence of the single iteration process of solving the system of one-dimensional problems (1.20)–(1.22) with a fixed number M of terms in the approximating expression and (ii) convergence of solution (1.5) with increasing number of approximating functions.

Whether these conditions are satisfied is checked by comparing two successive approximations.

The solution obtained with the EKM is validated against solutions obtained with other methods. Test examples are borrowed from [3, 16, 19] and selected so as to illustrate the features of the class of problems being considered such as the anisotropy of the material and the cantilever restraint of the parallelepiped. Since the natural frequencies of a cantilevered anisotropic parallelepiped were not calculated in [3], the solution for such boundary conditions is validated for an isotropic material using the results from [16, 19].

Example 1. Let us determine the natural frequencies of a rectangular parallelepiped $\Omega \cup \partial\Omega = \{x, y, z: x \in [0, a], y \in [0, a], z \in [0, c]\}$ with a square base made of a material with different types of anisotropy and the following elastic characteristics [3]:

Trigonal materials

$$[C] = \begin{bmatrix} 86.74 & 6.99 & 11.91 & -17.91 & 0 & 0 \\ & 86.74 & 11.91 & 17.91 & 0 & 0 \\ & & 107.2 & 0 & 0 & 0 \\ & \text{sym.} & & 57.94 & 0 & 0 \\ & & & & 57.94 & -17.91 \\ & & & & & 39.88 \end{bmatrix} \text{GPa}. \tag{2.1}$$

TABLE 1

Case	Frequency No.	Material	Boundary conditions	c/a	M
I	1	trigonal	CFCF (2.4)	0.5	4
II	2	monoclinic	SSSS (2.5)	0.1	3
III	3	orthotropic	CFCF (2.4)	0.5	2

Monoclinic materials

$$[C]=\begin{bmatrix} 86.74 & -8.25 & 27.15 & -3.66 & 0 & 0 \\ & 129.77 & -7.42 & 5.7 & 0 & 0 \\ & & 102.83 & 9.92 & 0 & 0 \\ & \text{sym.} & & 38.61 & 0 & 0 \\ & & & & 68.81 & 2.53 \\ & & & & & 29.01 \end{bmatrix} \text{GPa.} \tag{2.2}$$

Orthotropic materials

$$[C]=\begin{bmatrix} 160.0 & 37.3 & 1.72 & 0 & 0 & 0 \\ & 86.87 & 15.72 & 0 & 0 & 0 \\ & & 84.81 & 0 & 0 & 0 \\ & \text{sym.} & & 25.58 & 0 & 0 \\ & & & & 42.68 & 0 \\ & & & & & 42.06 \end{bmatrix} \text{GPa.} \tag{2.3}$$

Let us analyze the following boundary conditions: two opposite edges are clamped and the other two are free (CFCF in [3]):

$$u_1 = u_2 = u_3 = 0 \quad \text{at} \quad x = 0, a;$$
$$\sigma_{22} = \sigma_{21} = \sigma_{23} = 0 \quad \text{at} \quad y = 0,\ a; \tag{2.4}$$

and Navier boundary conditions at all edges (SSSS in [19]):

$$u_2 = u_3 = 0, \quad \sigma_{11} = 0 \quad \text{at} \quad x = 0,\ a;$$
$$u_1 = u_3 = 0, \quad \sigma_{22} = 0 \quad \text{at} \quad y = 0,\ a. \tag{2.5}$$

The planes $z = 0$ and $z = c$ are free from load: $\sigma_{33} = \sigma_{13} = \sigma_{23} = 0$ at $z = 0, c$.

We will illustrate the computational aspects (satisfaction of conditions (i), (ii) and comparison with other solutions) of the EKM for different frequencies, materials, boundary conditions, and dimensions of the parallelepiped. Table 1 summarizes the cases analyzed. Comparison is made using the frequency parameter $\tilde{\omega} = \omega c\sqrt{\rho / C_{11}}$ introduced in [3].

Table 2 collects frequencies illustrating the convergence of the single iteration process of solving the system of one-dimensional problems (1.20)–(1.22) (parameter j) at a fixed number M of approximating terms given in the last column of Table 1.

Table 2 indicates that four to seven iterations are required for the solution to converge in four decimal places at different number of approximating functions.

TABLE 2

Cases	*j*						
	1	2	3	4	5	6	7
I	0.9422	0.8637	0.8051	0.8028	0.8027	0.8026	0.8026
II	0.5276	0.5290	0.1260	0.1242	0.1242	0.1242	0.1242
III	0.7461	1.050	1.043	1.044	1.044	1.044	1.044

TABLE 3

Cases	*M*					
	1	2	3	4	5	6
I	0.9485	0.8049	0.8030	0.8026	0.8022	0.8022
II	0.1266	0.1260	0.1242	0.1242	0.1242	0.1242
III	1.059	1.044	1.042	1.041	1.041	1.041

Table 3 demonstrates how the natural frequencies converge depending on the number of terms in series (1.5).

It can be seen that the natural frequencies calculated by (1.4) converge in four decimal places with increase in the number of terms in (1.5) at no greater than six terms of approximation.

The natural frequencies calculated with the EKM and satisfying both conditions (i) and (ii) are validated by comparing them with those in [3] for the above types of anisotropy. These data are summarized in Tables 4 and 5 for the boundary conditions (2.4) and (2.5), respectively.

The difference between frequencies obtained by the finite-element method [3] and by our approach does not exceed 1%.

Example 2. To test the approach for a cantilevered parallelepiped, we will use the data from [16, 19] for an isotropic material. Comparison is made using the frequency parameter $\Omega_* = \omega b^2 \sqrt{\rho c / D}$ introduced in [19] ($D = Ec^3 / 12(1-\mu^2)$, E is Young's modulus, μ is Poisson's ratio).

Assume that the edge $x = 0$ is clamped and the other edges are free:

$$u_1 = u_2 = u_3 = 0 \quad \text{at} \quad x = 0,$$

$$\sigma_{11} = \sigma_{12} = \sigma_{13} = 0 \quad \text{at} \quad x = a,$$

$$\sigma_{22} = \sigma_{21} = \sigma_{23} = 0 \quad \text{at} \quad y = 0, b,$$

$$\sigma_{33} = \sigma_{13} = \sigma_{23} = 0 \quad \text{at} \quad z = 0, c. \tag{2.6}$$

How conditions (i) and (ii) are satisfied to solve the problem with the EKM using these boundary conditions is illustrated by Table 6 (convergence of the general iteration process of solving the system of one-dimensional problems (1.20)–(1.22) with a fixed number of approximation terms) and Table 7 (convergence of the solution depending on the number of approximation terms).

TABLE 4

Anisotropy	Frequency No.	$c / a = 0.5$		$c / a = 0.1$	
		EKM	[3]	EKM	[3]
trigonal	1	0.8020	0.8005	0.05950	0.05950
	2	0.9907	0.9795	0.07160	0.07150
	3	1.026	1.025	0.1.145	0.1141
monoclinic	1	0.8259	0.8241	0.05980	0.05980
	2	0.09862	0.9800	0.06990	0.06980
	3	1.025	1.023	0.1184	0.1178
orthotropic	1	0.6812	0.6821	0.05850	0.05850
	2	0.7436	0.7436	0.09480	0.09480
	3	1.041	1.042	1.472	1.472

TABLE 5

Anisotropy	Frequency No.	$c / a = 0.5$		$c / a = 0.1$	
		EKM	[3]	EKM	[3]
trigonal	1	0.9252	0.9210	0.05350	0.05350
	2	1.018	1.017	0.1298	0.1296
	3	1.056	1.051	0.1984	0.1984
monoclinic	1	0.9055	0.9036	0.05270	0.05270
	2	0.9075	0.9064	0.1243	0.1241
	3	0.9373	0.9299	0.1426	0.1424
orthotropic	1	0.7293	0.7295	0.04770	0.04770
	2	0.8054	0.8054	0.1021	0.1021
	3	0.8054	0.8054	0.1227	0.1227

TABLE 6

c/a	Frequency No.	M	j						
			1	2	3	4	5	6	7
0.5	1	2	2.957	2.952	2.950	2.950	2.950	2.950	2.950
	3	3	5.233	5.222	5.215	5.205	5.204	5.204	5.204
0.1	2	3	8.111	8.107	8.102	8.099	8.091	8.090	8.090
	3	4	3.773	7.187	16.89	20.26	20.18	20.17	20.17

TABLE 7

c/a	Frequency No.	j					
		1	2	3	4	5	6
0.5	1	3.118	2.950	2.938	2.934	2.933	2.933
	3	5.340	5.237	5.204	5.197	5.193	5.193
0.1	2	8.362	8.114	8.090	8.079	8.071	8.071
	3	22.03	20.72	20.19	20.17	20.17	20.17

As with anisotropic materials and conditions (2.4) and (2.5), four to seven iterations are sufficient for the solution for a cantilevered parallelepiped to converge in four decimal places. Stable values of frequencies are obtained with five to six approximation terms.

Table 8 compares the results with those from [16, 19] where the natural frequencies were calculated with the Ritz method using, as a basis, B-spline functions and orthogonal polynomials, respectively.

The frequencies calculated with different approaches differ by less than 1%.

Thus, testing the approach (examples 1 and 2) indicates that it works well for anisotropic materials and various boundary conditions.

3. Analysis of the Natural Frequencies of an Anisotropic Parallelepiped. Let us use the above approach to calculate the lower natural frequencies of a cantilevered parallelepiped. We will examine the dependence of the frequencies on the properties of the anisotropic material and the contribution of the secondary stiffnesses relating tensile/compressive strains and shear strains.

Let the edge $x = 0$ of the parallelepiped be clamped and the other edges be free (boundary conditions (2.6)). The length a of the parallelepiped along the Ox-axis is constant, while the relative dimensions of the cross-section $x = \text{const}$ with constant area $S = b \times c = \text{const}$ vary, which is characterized by the parameter $\alpha = c / b$.

The parallelepiped is made of a unidirectional composite reinforced with CFRP carbon fibers,

$$E_1 = 2.11E_0, \quad E_2 = E_3 = 0.053E_0, \quad G_{12} = G_{13} = 0.026E_0, \quad G_{23} = 0.013E_0,$$

$$\mu_{21} = 0.25, \quad \rho = \rho_0 = 1524 \text{ kg/m}^3, \quad E_0 = 10^{11} \text{ N/m}^3. \tag{3.1}$$

The axes of symmetry of the orthotropic material are initially aligned with the geometrical axes of the body, i.e., E_1, E_2, and E_3 correspond to the Ox-, Oy-, and Oz-axes, respectively. The change in the angle φ in the plane xy between the physical and

TABLE 8

Frequency No.	$c/a = 0.5$			$c/a = 0.1$		
	EKM	[19]	[16]	EKM	[19]	[16]
1	2.9327	2.9331	2.9372	3.4400	3.4387	3.4480
2	4.3889	4.3865	4.3910	8.0706	8.0746	8.0996
3	5.1926	5.1925	5.1944	20.170	20.152	20.209

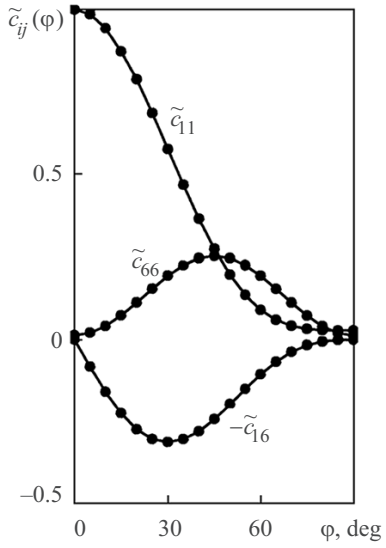

Fig. 1

geometrical axes of the parallelepiped allows considering it as structurally anisotropic with one plane of elastic symmetry perpendicular to the *Oz*-axis. The elements of the matrix of Hooke's law $\overline{\sigma} = C\overline{\varepsilon}$ for orthotropic material (three planes of elastic symmetry $C^o = \{c_{ij}^o\}$) and for anisotropic material (one plane of elastic symmetry $C = \{c_{ij}\}$) are related as follows, depending on the angle φ [2]:

$$c_{11} = c_{11}^o \cos^4\varphi + 2(c_{12}^o + 2c_{66}^o)\sin^2\varphi\cos^2\varphi + c_{22}^o \sin^4\varphi,$$

$$c_{22} = c_{11}^o \sin^4\varphi + 2(c_{12}^o + 2c_{66}^o)\sin^2\varphi\cos^2\varphi + c_{22}^o \sin^4\varphi,$$

$$c_{12} = c_{12}^o + [c_{11}^o + c_{22}^o - 2(c_{12}^o + 2c_{66}^o)]\sin^2\varphi\cos^2\varphi,$$

$$c_{66} = c_{66}^o + [c_{11}^o + c_{22}^o - 2(c_{12}^o + 2c_{66}^o)]\sin^2\varphi\cos^2\varphi,$$

$$c_{16} = 0.5[c_{22}^o \sin^2\varphi - c_{11}^o \cos^2\varphi + (c_{12}^o + 2c_{66}^o)\cos 2\varphi]\sin 2\varphi,$$

$$c_{26} = 0.5[c_{22}^o \cos^2\varphi - c_{11}^o \sin^2\varphi - (c_{12}^o + 2c_{66}^o)\cos 2\varphi]\sin 2\varphi,$$

$$c_{44} = c_{44}^o \cos^2\varphi + c_{55}^o \sin^2\varphi, \quad c_{55} = c_{44}^o \sin^2\varphi + c_{55}^o \cos^2\varphi,$$

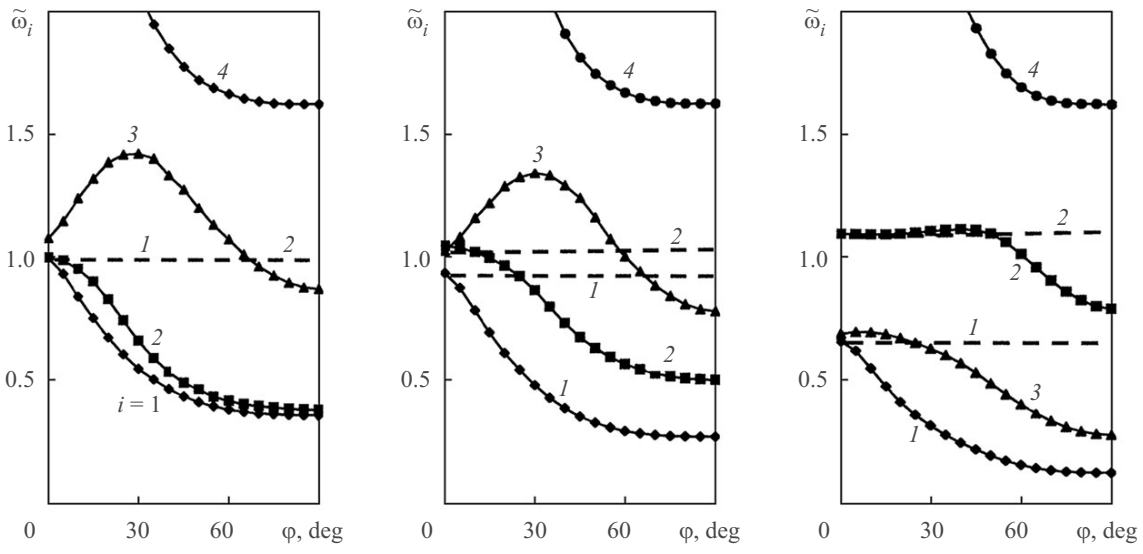

Fig. 2

$$c_{45} = (c_{44}^o - c_{55}^o)\sin\varphi\cos\varphi, \quad c_{13} = c_{13}^o \cos^2\varphi + c_{23}^o \sin^2\varphi,$$

$$c_{23} = c_{13}^o \sin^2\varphi + c_{23}^o \cos^2\varphi, \quad c_{36} = (c_{23}^o - c_{13}^o)\sin\varphi\cos\varphi, \quad c_{33} = c_{33}^o. \tag{3.2}$$

Figure 1 shows, as an illustration, the stiffness characteristics $\widetilde{c}_{11} = \widetilde{c}_{11}(\varphi)$, $\widetilde{c}_{66} = \widetilde{c}_{66}(\varphi)$, $\widetilde{c}_{16} = \widetilde{c}_{16}(\varphi)$, $\varphi \in [0°, 90°]$, which give an indication of the elements of the matrix $C = \{c_{ij}\}$ $(i, j = \overline{1, 6})$ $(\widetilde{c}_{ij}(\varphi) = c_{ij}(\varphi) / c_{11}(0))$, considering the symmetry and periodicity of transformations (3.2).

Calculations were carried out in two stages. At the first stage, we calculated the lower frequencies of an anisotropic parallelepiped depending on the orientation of composite fibers (3.1) ($\varphi \in [0°, 90°]$) for three relative dimensions of the section $x = \text{const}$: $\alpha = 1$, 0.5, 0.1 ($\alpha = 1$ corresponds to a cantilevered parallelepiped with a square cross-section; $\alpha = 0.1$ to a plate of thickness c and dimensions $a \times b$).

The first four frequencies $\widetilde{\omega}_i = \omega_i / \omega_{1,\alpha=1}(0)$ $(i = 1, 2, 3, 4)$ divided by the minimum frequency of the orthotropic parallelepiped with square cross-section $x = \text{const}$ ($\varphi = 0$, $\alpha = 1$) are presented in Fig. 2*a*, *b*, *c* for $\alpha = 1$, 0.5, 0.1 ($a = 25l_0$, $S = 100l_0^2$, l_0 is a typical length scale). If the displacements along the *Ox*-axis do not reverse sign, these frequencies correspond to the following vibration modes: (i) predominantly bending vibrations along the *Oz*-axis (each cross-section x = const of the parallelepiped shifts along this axis as a rigid-body), (ii) predominantly bending vibrations along the *Oy*-axis, (iii) shear vibrations in the plane x = const; (iv) piston-like vibrations along the *Ox*-axis.

The curves $\widetilde{\omega}_i = \widetilde{\omega}_i(\varphi)$ for the parallelepiped with square cross-section $x = \text{const}$ are monotonically decreasing for all frequencies, except for the third one (curves *1*, *2*, *4* in Fig. 2). Their qualitative behavior is similar to that of the stiffness $\widetilde{c}_{11}$, which dominates over the other stiffnesses for these vibration modes (Fig. 1). For the third frequency (curve *3*), the curve $\widetilde{\omega}_i = \widetilde{\omega}_i(\varphi)$ is nonmonotonic, peaking at $\varphi = 30°$. The qualitative behavior of this curve follows that of the stiffness $\widetilde{c}_{66}$, which together with $\widetilde{c}_{12}$, is predominant in determining shear strains (Fig. 1). The 15% difference between the first two frequencies is observed within $\varphi \in [10°, 30°]$. It is this quantity that is responsible for the anisotropic effect. In the isotropic case, both first frequencies are equal and independent of the angle φ (dashed lines in Figs. 1 and 2).

For the other dimensions of the cross-section $x = \text{const}$ ($\alpha = 0.5$, 0.1), the qualitative behavior of $\widetilde{\omega}_i = \widetilde{\omega}_i(\varphi)$ hardly changes (Fig. 2*b*, *c*). The quantitative difference between the first and second frequencies substantially increases, which is caused by the change in the dimensions of the parallelepiped rather than by the anisotropy of the material. The frequency curves $\widetilde{\omega}_1 = \widetilde{\omega}_1(\varphi)$ (bending vibrations along the *Oz*-axis) decrease with the parameter α for all material characteristics considered. The curves $\widetilde{\omega}_2 = \widetilde{\omega}_2(\varphi)$ for the second frequency, conversely, tend to increase, while the curves $\widetilde{\omega}_3 = \widetilde{\omega}_3(\varphi)$ not only decrease, but

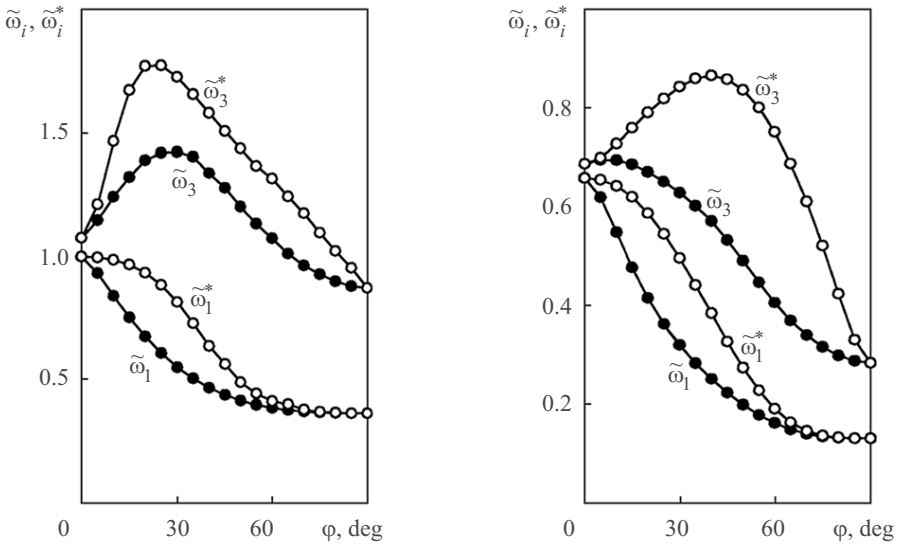

a *b*

Fig. 3

also become more shallow. For the thick plate with $\alpha = 0.1$ (Fig. 2*c*), the frequencies $\tilde{\omega}_2 = \tilde{\omega}_2(\varphi)$ hardly change up to $\varphi = 45°$ and are higher than the frequencies of shear vibrations, $\tilde{\omega}_2(\varphi) > \tilde{\omega}_3(\varphi)$, over the entire range of φ.

The frequencies of piston-like vibrations (curve *4*) notably increase in the range $\varphi \in [0, 20°]$ with decrease in α and are almost independent of this parameter for $\varphi > 60°$.

The secondary stiffnesses were allowed for at the second stage of calculations. We compared the curves $\tilde{\omega}_i = \tilde{\omega}_i(\varphi)$ and $\tilde{\omega}_i^* = \tilde{\omega}_i^*(\varphi)$ obtained with (exact scheme) and without (conventionally simplified orthotropic scheme) regard to the stiffnesses c_{16}, c_{26}, c_{45} in Hooke's law. These results are presented in Fig. 3 for the first and third frequencies of parallelepipeds of square ($\alpha = 1$, Fig. 3*a*) and rectangular ($\alpha = 0.1$, Fig. 3*b*) cross-section $x = \text{const}$.

As can be seen, the qualitative behavior of the frequency curves $\tilde{\omega}_i = \tilde{\omega}_i(\varphi)$ and $\tilde{\omega}_i^* = \tilde{\omega}_i^*(\varphi)$ does not change for both frequencies. The orthotropic scheme naturally overestimates them. The simplified scheme introduces a larger error ($\varepsilon_i(\varphi) = (\tilde{\omega}_i^*(\varphi) - \tilde{\omega}_i(\varphi))/\tilde{\omega}_i(\varphi) \times 100, i = 1, 3$) into the first frequency (~50% for $\alpha = 1$ and $\alpha = 0.1$) than into the third frequency (~20% for $\alpha = 1$ and 45% for $\alpha = 0.1$).

Conclusions. 1. Our approach to determining the natural frequencies of an elastic parallelepiped using a three-dimensional problem statement has been tested for various anisotropic materials (trigonal, monoclinic, orthotropic) and validated against results obtained with the finite-element and Ritz methods.

2. The influence of the properties of anisotropic materials on the lower frequencies of a cantilevered parallelepiped has been analyzed. It has been shown that the lower frequencies of the cantilevered parallelepiped follow the variation in the predominant stiffness characteristics, which is not so for other boundary conditions.

3. Neglecting the secondary stiffnesses that relate the tensile/compressive strains and the shear strains in Hooke's law results in a natural overestimation of the frequencies. The qualitative behavior of the curves does not change, while the quantitative differences may exceed 50% in some cases.

REFERENCES

1. Von L. Collatz, *Eigenvalue Problems with Engineering Applications* [in German], Akad. Verlagsges., Leipzig (1963).
2. S. G. Lekhnitskii, *Theory of Elasticity of an Anisotropic Body*, Mir, Moscow (1981).
3. R. C. Barta, L. F. Qian, and L. M. Chen, "Natural frequencies of thick square plates made of orthotropic, trigonal, monoclinic, hexagonal and triclinic materials," *J. Sound Vibr.*, **270**, No. 4–5, 1074–1086 (2004).

4. E. I. Bespalova, ”Solving stationary problems for shallow shells by a generalized Kantorovich–Vlasov method,” *Int. Appl. Mech.*, **44**, No. 11, 1283–1293 (2008).
5. E. I. Bespalova and G. P. Urusova, “Solving the torsion problem for an anisotropic prism by the advanced Kantorovich–Vlasov method,” *Int. Appl. Mech.*, **46**, No. 2, 149–158 (2010).
6. E. I. Bespalova, “Determining the natural frequencies of an elastic parallelepiped by the advanced Kantorovich–Vlasov method,” *Int. Appl. Mech.*, **47**, No. 4, 410–421 (2011).
7. E. I. Bespalova and G. P. Urusova, “Solution of the Lame problem by the complete systems method,” *Int. J. Comp. Meth. in Eng. Sci. Mech.*, **14**, No. 2, 159–167 (2013).
8. P. M. Ciancio, C. A. Rossit, and P. A. A. Laura, ”Approximate study of the free vibrations of a cantilever anisotropic plate carrying a concentrated mass,” *J. Sound Vibr.*, **302**, No. 3, 621–628 (2007).
9. G. M. Cook and A. Tessler, ”A {3, 2}-order bending theory for laminated composite and sandwich beams,” *Composites Part B: Engineering*, **29**, No. 5, 565–576 (1998).
10. D. J. Gorman and R. Singhal, ”Free vibration analysis of cantilever plates with step discontinuities in properties by the method of superposition,” *J. Sound Vibr.*, **253**, No. 3, 631–652 (2002).
11. A. Ya. Grigorenko and T. L. Efimova, ”Free axisymmetric vibrations of solid cylinders: numerical problem solving,” *Int. Appl. Mech.*, **46**, No. 5, 499–508 (2010).
12. Ya. M. Grigorenko and A. Ya. Grigorenko, ”Static and dynamic problems for anisotropic inhomogeneous shells with variable parameters and their numerical solution (review),” *Int. Appl. Mech.*, **49**, No. 2, 123–193 (2013).
13. Ya. M. Grigorenko, A. S. Bergulev, and S. N. Yaremchenko, ”Numerical solution of bending problems for rectangular plates,” *Int. Appl. Mech.*, **49**, No. 1, 81–94 (2013).
14. A. Houmat, ”Three-dimensional free vibration analysis of plates using the h-p version of the finite-element method,” *J. Sound Vibr.*, **290**, No. 3–5, 690–704 (2006).
15. R. Li, Y. Zhong, B. Tian, and J. Du, ”Exact bending solutions of orthotropic cantilever thin plates subjected to arbitrary loads,” *Int. Appl. Mech.*, **47**, No. 1, 131–143 (2011).
16. K. M. Liew, K. C. Hung, and K. M. Lim, ”A continuum three-dimensional vibration analysis of thick rectangular plates,” *Int. J. Solids Struct.*, **30**, 3357–3379 (1993).
17. V. A. Maximyuk, E. A. Storozhuk, and I. S. Chernyshenko, ”Variational finite-difference methods in linear and nonlinear problems of the deformation of metallic and composite shells (review),” *Int. Appl. Mech.*, **48**, No. 6, 613–687 (2012).
18. O. G. McGee and G. T. Giaimo, “Three-dimensional vibrations of canilevered right triangular plates,” *J. Sound Vibr.*, **159**, No. 2, 279–293 (1992).
19. I. H. Nagino, T. Mikami, and T. Mizusawa, ”Three-dimensional free vibration analysis of isotropic rectangular plates using the B-spline Ritz method,” *J. Sound Vibr.*, **317**, No. 1–2, 329–353 (2008).
20. L. Woodcock Roland, B. Bhat Rama, and G. Stiharu Ion, ”Effect of ply orientation on the in-plane vibration of single-layer composite plates,” *J. Sound Vibr.*, **312**, No. 1–2, 94–108 (2008).
21. Xiang Song, Yang Ming-sui, Jiang Shao-xi, and Wang Ke-ming, “Three-dimensional vibration analysis of isotropic plates by multiquadric and thin-plate spline radial basis functions,” *Comp. & Struct.*, **88**, No. 13–14, 837–844 (2010).
22. Zhou Ding, Liu Weiqing, and Yang Qingli, “Three-dimensional vibration analysis of cantilevered skew plates,” *J. Sound Vibr.*, **313**, No. 1–2, 134–148 (2008).